Simultaneous Binding and Bending of Promoter DNA by the TATA Binding Protein: Real Time Kinetic Measurements†

Kay M. Parkhurst,‡ Michael Brenowitz,§ and Lawrence J. Parkhurst*,‡

Department of Chemistry, University of Nebraska, Lincoln, Nebraska 68588-0304, and Department of Biochemistry, Albert Einstein College of Medicine, Bronx, New York 10461

Received December 21, 1995; Revised Manuscript Received April 1, 1996⊗

ABSTRACT: The binding and bending of tetramethylrhodamine−5′-(GGGC**TATAAAAG**GG)$_{duplex}$-3′−fluorescein by native *Saccharomyces cerevisiae* TATA binding protein (TBP) have been investigated using fluorescence resonance energy transfer. Probability distributions derived from fluorescein emission lifetime measurements show a decrease in the mean 3′-fluorescein−5′-rhodamine distance from 56.5 to 46.8 Å upon binding of the oligomer to TBP, consistent with the DNA bend observed by X-ray crystallography. The kinetics, monitored in real time using stopped flow fluorimetry, demonstrate simultaneous binding and bending of a TATA box by TBP with a single second-order rate constant of $(2.4 \pm 0.3) \times 10^6$ M^{-1} s^{-1} at 30 °C.

Biochemical and crystallographic studies have demonstrated that the binding of the TATA binding protein (TBP[1]) to the minor groove of a TATA promoter element results in the unwinding and bending of the DNA duplex (Starr & Hawley, 1991; Lee et al., 1991; Horikoshi et al., 1992; Kim, J. L., et al., 1993; Kim, Y., et al., 1993; Kim & Burley, 1994). The rate of association of TBP with promoter sequences proceeds as a second-order reaction at rates significantly slower than diffusion-limited (Hoopes et al., 1992; Kuddus & Schmidt, 1993; Perez-Howard et al., 1995; Brenowitz et al., 1995). The magnitude of the TBP-induced bend in solution, as measured by the electrophoretic circular permutation assay, is dependent upon the sequence of the TATA box and has been correlated with the rate of dissociation of the TBP−promoter complex (Starr et al., 1995). The thermodynamic relationship relating DNA binding and bending has been elucidated using the *Escherichia coli* protein CAP as a model system (Kahn & Crothers, 1992; Kahn et al., 1994). In essence, if protein binding bends the DNA, the protein will have increased affinity for "prebent" DNA. Such a relationship has been demonstrated for TBP (Parvin et al., 1995). However, the magnitudes of the DNA bends observed in cocrystal structures of *Arabidopsis thaliana* TBP complexed with a series of DNA sequences (including several analyzed in the above-referenced circular permutation studies) are identical to those observed in the original *Arabidopsis* TBP cocrystal structure using the adenovirus major late promoter (S. Burley, personal communication). It should also be noted that the DNA bend observed in the *Arabidopsis* TBP cocrystal structure is identical to that observed in the cocrystal structure of the C-terminal domain of *Saccharomyces cerevisiae* TBP (Kim, Y., et al., 1993).

Thus, the mechanism of sequence-specific binding by TBP and the relationship between promoter binding and DNA bending remain unresolved. In particular, what role does DNA bending play in the mechanism of promoter recognition by TBP? We have addressed directly the issue of stepwise or simultaneous DNA binding and bending by monitoring the interaction in solution of the native *S. cerevisiae* TBP with the major late promoter using the steady state and time-resolved fluorescence emission of a doubly labeled 14-mer oligonucleotide with 5′-bound tetramethylrhodamine and 3′-bound fluorescein. The dyes acted as a donor/acceptor pair for Förster resonance energy transfer (FRET) and thus provided a very sensitive measure of the distance between the 3′- and 5′-ends of the helix. Previously published studies of a similarly doubly labeled 16-mer (Parkhurst & Parkhurst, 1995a,b) provide the foundation for these protein−DNA studies. The reported results include a detailed consideration of Förster energy transfer between dyes covalently bound to either end of a DNA oligomer. The 3′−5′ distances and the distance distributions were determined for the labeled oligomer alone and bound to TBP using fluorescence lifetime measurements. Time-dependent measurements of the steady state fluorescence obtained by stopped flow fluorimetry demonstrated that DNA bending occurs simultaneously with binding of TBP to the promoter DNA.

MATERIALS AND METHODS

Protein. The TBP used in these studies was prepared as described (Petri et al., 1995) except that cell lysis was conducted in a buffer containing 1 M KCl and 1 M ammonium acetate in addition to the published components. The TBP stock solution of 53.5 mM was stored as has been described (Petri et al., 1995).

DNA Probes. The sequence of the doubly labeled DNA 14-mer used in these studies was based on that of the

† This work was supported by NIH Grants GM51506 (M.B.) and DK36288 (L.J.P.).

* To whom correspondence should be addressed: Department of Chemistry, University of Nebraska, Lincoln, NE 68588-0304.

‡ University of Nebraska.

§ Albert Einstein College of Medicine.

⊗ Abstract published in *Advance ACS Abstracts,* May 1, 1996.

[1] Abbreviations: TBP, TATA binding protein; FRET, Förster resonance energy transfer. All oligomers are deoxyribonucleotides: 14*F and 14*F_{dpx}, 5′-GGGCTATAAAAGGG-3′ with 3′-bound fluorescein, single strand and duplex, respectively; and R*14*F and R*-14_{dpx}*F, 5′-GGGCTATAAAAGGG-3′ with 5′-bound tetramethylrhodamine and 3′-bound fluorescein, single strand and duplex, respectively.

S0006-2960(95)03030-3 CCC: $12.00

adenovirus major late promoter: tetramethylrhodamine−5′-GGGC**TATAAAAG**GG-3′−fluorescein (R*14*F). The singly labeled 14-mer (14*F) was identical except it had no 5′-bound tetramethylrhodamine. Both labeled oligomers were from Research Genetics (Huntsville, AL). The complementary 14-mer was from the UNL departmental DNA/RNA synthesis facility. The 5′- and 3′-linkages between the dyes and the oligomer were identical to those reported previously (Parkhurst & Parkhurst, 1995a). Probe concentrations were determined as described previously (Parkhurst & Parkhurst, 1995a) and confirmed by titration of R*14*F with the complementary oligonucleotide, monitoring steady state fluorescence emission. The stock solutions of DNA were stored at −80 °C at the following concentrations: 1−2 mM, R*14*F; 2.25 mM, 14*F; and 4.5 mM, complementary strand. All steady state, lifetime, and kinetic studies were conducted at 30 °C in pH 7.4 Tris/HCl buffer containing 100 mM KCl, 2.5 mM $MgCl_2$, and 1 mM $CaCl_2$.

Instrumentation. Absorbance spectra were collected on a Hewlett-Packard diode array spectrophotometer (model HP8452A). The steady state fluorimeter (Photon Technology International, Inc., model A-1010), the SLM-Aminco multiharmonic frequency phase fluorometer (model 4850), and associated data acquisition were as described elsewhere (Parkhurst & Parkhurst, 1995a), except the excitation light source was the 488 nm line from a Coherent argon ion laser (model INNOVA 70-4, Santa Clara, CA), with 8−10 mW of light incident on the sample. The stopped flow apparatus and data acquisition are also as described elsewhere (Martin & Parkhurst, 1989), with the following refinements. The excitation light source was the 488 nm line of a Lexel (model 75) argon ion laser, with 6−8 mW incident on the cuvette. The beam passed directly through the center of the cuvette and probed ∼50% of the solution volume. The photocathode of the emission photomultiplier was situated directly over the cuvette, which was masked to minimize scattered light and was immediately preceded by a 520 nm interference filter (Oriel Corp., Stratford, CT). The mechanical components of the apparatus had been retooled just prior to these studies in order to achieve precise alignment throughout. A low friction bushing for the plunger of the stopping syringe was added, and a small magnet was fixed to the far end of that plunger. This magnet was aligned 0.2 mm from a strong magnet (Edmund Scientific) on an adjustable mount in order to ensure a precise stop point. A simple electrical circuit between the stop-nut of the stopping syringe plunger and the brass stopping block monitored flow concurrently with acquisition of the fluorescence emission data and signaled the precise time of the flow termination. The instrument dead time (defined here as the time required to fill the cuvette to one-half of its total volume just prior to the cessation of flow) was determined by attaching a linear potentiometer to the syringe plunger. The voltage output from the potentiometer is proportional to distance travelled by the shaft and was recorded as a function of time upon firing the piston. The final flow velocity of the plunger was determined from this curve and was used with the relationship between syringe volume and distance traveled to calculate the dead time. The sample temperature within all three fluorescence instruments was thermostatted using a Lauda K-2/R constant temperature circulating water bath. For the steady state and lifetime instruments, preliminary temperature measurements were made with a thermistor placed directly in buffer in the cuvette to determine the water bath setting needed to achieve 30 °C. For the stopped flow work, the temperature was continuously monitored by a thermistor in the small water chamber surrounding the cuvette.

Steady State Measurements. Steady state measurements were made for the single strand (R*14*F), free duplex (R*14_{dpx}*F), and TBP-bound duplex in order to observe differences in the fluorescein emission as a result of changes in the 3′−5′ distance. For these experiments, R*14*F was diluted into 250 mL of buffer in a short semi-microcuvette to a final concentration of 20 nM. To form the DNA duplex, unlabeled complement was added to a final concentration of 25 nM, and sufficient time was allowed for essentially complete duplex formation. Scans were collected every 0.25 nm from 500 to 600 nm, and an initial scan of the buffer alone, which included the Raman scattering from water, was subtracted from all subsequent scans.

To obtain an equilibrium constant for binding of the R*14_{dpx}*F to TBP, the protein was added to the duplex to final concentrations of 20, 50, 120, 224, 1000, and 1967 nM. A new aliquot of a 20 nM R*14_{dpx}*F solution was used for each TBP concentration, and scans were collected after several minutes of equilibration; this approach avoided denaturation of the protein from repeated stirring following multiple additions. The determination of the fraction of bound R*14_{dpx}*F at each TBP concentration and the analysis used to obtain a value for the equilibrium constant have been described [Parkhurst and Parkhurst (1995a) and Parkhurst et al. (1994), respectively].

For the probe containing only the fluorescein label, duplex was formed using 5 nM 14*F and 10 nM complement, and the emission spectrum was scanned from 500 to 550 nm. TBP was added to the 14_{dpx}*F to 320, 480, and 640 nM. An equilibrium constant for the TBP−promoter interaction was not determined for this probe.

Fluorescence Lifetime Measurements. Probability distributions [$P(R)$] of the 3′−5′ distance for the free and TBP-bound R*14_{dpx}*F were derived from measurements of the fluorescein emission lifetime (Cheung, 1991; Lakowicz et al., 1988). For these measurements, the total solution volume was 2 mL and the concentrations of R*14*F and complement were 150 and 200 nM, respectively. Phase shift and modulation measurements were made from 4 to 208 MHz in 4 MHz increments. Twenty-five successive measurements were averaged to obtain a data set, and four such sets were collected for the R*14_{dpx}*F. TBP was then added to a final concentration of 275 nM, and three additional data sets were collected. A second addition of TBP was made to a final total concentration of 410 nM, and two more data sets were collected. For the singly labeled oligomer, the above procedure was repeated exactly as described except that 14*F was substituted for R*14*F.

Each of the data sets was fit to mono-, bi-, and triexponential decay models using the SLM software as described previously (Parkhurst & Parkhurst, 1995b), to obtain the α and τ values that best described the fluorescence decay. Since the α and τ values for each group of data sets were virtually identical, only the set in each group with the best χ^2 value was further analyzed for the mean distance between the 5′- and 3′-dyes on the DNA probe and for the probability distribution [$P(R)$] over which that distance varied. In these analyses, the fluorescein decay of the donor in the presence of an acceptor (R*14_{dpx}*F) is compared to that of the donor

only (14_{dpx}*F), to retain only those changes that derive from FRET. The analyses were conducted as described in detail previously (Parkhurst & Parkhurst, 1995b). The errors in the distance distribution parameters σ and $\bar{R}$ were determined as follows. The root mean square (rms) residual was determined at each frequency for the sine and cosine Fourier transforms of the fitted data sets from the errors in the phase and modulation vectors using error propagation theory; these rms residuals were used to construct 25 Gaussian-distributed noise vectors over the frequency domain for the sine and cosine transforms. The noise vectors were added to the sine and cosine transform vectors obtained using the optimal values of σ and $\bar{R}$, and the resulting 25 simulated data sets were fit by least squares for σ and $\bar{R}$. The results were used to estimate the standard deviations for the distributions of σ and $\bar{R}$.

Stopped Flow Fluorimetry. The kinetic course of the TBP−promoter association reaction was monitored as a function of time and [TBP] using the stopped flow fluorimeter, by flowing R*14_{dpx}*F against TBP and monitoring the steady state emission of the fluorescein. For the stopped flow kinetic measurements, R*14*F and complement were diluted into buffer to final concentrations of 40 and 80 nM, respectively, in 2 mL aliquots. Three 2 mL solutions of TBP were prepared, diluting stock TBP into buffer to final concentrations of 275, 550, and 1650 nM. (The concentration of each solution was halved after mixing in the stopped flow instrument.) These relative concentrations of R*14_{dpx}*F and TBP were such that the binding reactions could be analyzed using the pseudo-first-order approximation. The solutions of duplex and TBP were introduced into the drive syringes and allowed to thermally equilibrate (∼1 min as determined independently using a thermistor in the drive syringe) and the measurements made. Two thousand data points were collected in each experiment; the time constant for the emission photomultiplier was ≤0.1 times the time interval between points. For the 275 and 1650 nM solutions, data were collected for 81 and 12 s, respectively. For the 550 nM solution, measurements were made in two widely separated time frames, 0−409 ms and 0−40 s. A background photomultiplier voltage for buffer plus TBP was recorded immediately prior to each set of measurements.

Since significant photobleaching of the fluorescein occurred during the course of the stopped flow experiments, the R*14_{dpx}*F−TBP data were analyzed by first subtracting the change in emission due only to photobleaching and then obtaining from the corrected data the rate constant for R*14_{dpx}*F−TBP binding. The raw data sets were all composed initially of 2000 points; some data sets were truncated (to a minimum of 1700 points) to eliminate fluctuations in the laser intensity that occurred with the single beam instrument during the long time intervals. (Curves showing a significant fluctuation in laser intensity prior to the collection of 1700 points were rejected.) The data were normalized after first subtracting from each point the base line voltage. It was clear from preliminary work that the second half of each normalized curve represented a change in fluorescein emission due only to photobleaching. To obtain an exact value for each curve for the photobleaching rate constant, k_{bleach}, the last half of the data points was used to construct a linear plot of ln(fluorescence emission intensity) vs time; the plot was fit by linear regression, and a value for k_{bleach} was obtained from the slope of the fitted line. This value of k_{bleach} was used to extrapolate the second half of the data vector (representing photobleaching) back to time zero, and that extrapolated photobleaching curve was subtracted from the normalized kinetic curve. The remainder represented changes in emission intensity due only to the interaction of the R*14_{dpx}*F with TBP (and a negligible contribution from photobleaching of the fluorescein in the duplex prior to TBP binding). A second plot of ln(fluorescence emission intensity) vs time was constructed from this corrected curve, out to $4t_{1/2}$, and the data were fit by a linear regression. A value for the pseudo-first-order rate constant for R*14_{dpx}*F binding to TBP was obtained from the slope of the fitted line. A total of seven reaction curves were analyzed in this way, three curves with 825 nM TBP and two curves each with 138 and 275 nM TBP.

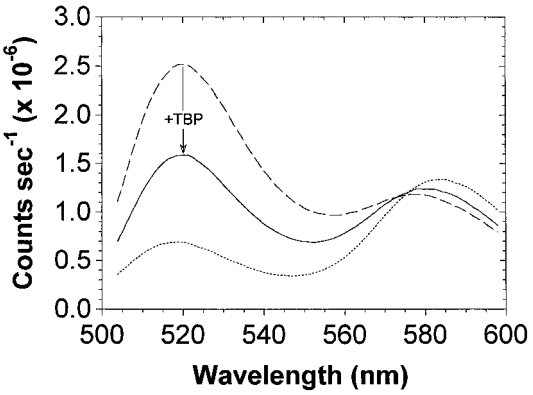

FIGURE 1: Steady state emission scans of 20 nM R*14_{dpx}*F as a single strand (···) and in a duplex both free in solution (− −) and bound to TBP (275 nM total, —). Direct absorption of the 488 nm excitation light gave rise to the 520 nm fluorescein emission peak; this emission was decreased by the resonant transfer of energy to the acceptor rhodamine. The 580 nm rhodamine emission peak derived both from direct absorption of the 488 nm excitation light, which is a constant background, and from the resonance transfer of energy from the donor fluorescein.

The singly labeled duplex was formed by diluting 14*F and complement into buffer to final concentrations of 30 and 65 nM, respectively. This solution was made to flow against a 550 nM solution of TBP. Data were collected in two time frames, 0−614 ms and 0−40 s. To obtain data for photobleaching of fluorescein in the TBP-bound 14_{dpx}*F, the probe and protein were made to flow together in the dark and allowed to equilibrate; the shutter was then opened, and data were collected for 40 s.

RESULTS

The differences in the 3′−5′ distance for the single strand (R*14*F), free duplex (R*14_{dpx}*F), and TBP-bound duplex were clearly reflected in the steady state fluorescence emission scans (Figure 1). Significant FRET occurred in the flexible single strand, resulting in decreased fluorescein emission and increased rhodamine emission. Formation of the less flexible duplex, upon addition of the complementary strand, separated the dyes, resulting in a decrease in FRET. Subsequent binding of the duplex to a saturating concentration of TBP increased FRET relative to the free duplex, resulting in a 37 ± 1% decrease in fluorescein emission. This result is consistent with the TBP-induced DNA bend bringing the 3′- and 5′-ends of the duplex closer together. Titration of the R*14_{dpx}*F with TBP resulted in incremental decreases in the 520 nm peak and correlated increases in

Table 1: Values of α and τ That Describe the Fluorescein Lifetime for the Free and TBP-Bound R*14_{dpx}*F and 14_{dpx}*F[a]

14-mer	α_1	τ_1 (ns)	α_2	τ_2 (ns)	χ^2
14_{dpx}*F	0.467	0.930	0.533	3.364	0.120
14_{dpx}*F−TBP	0.449	0.664	0.551	3.237	0.605
R*14_{dpx}*F	0.618	0.617	0.382	1.882	0.619
R*14_{dpx}*F−TBP	0.838	0.382	0.162	1.999	0.870

[a] The lifetimes are all well-described as biexponential decays and are essentially unchanged for [TBP] > 275 nM. Fluorescence lifetimes were measured in the frequency domain and analyzed for $P(R)$ as described previously (Parkhurst & Parkhurst, 1995b). The lifetime of the fluorescein in the 14_{dpx}*F changed slightly upon binding to the TBP, due to a change in the local environment of the fluorescein.

the 580 nm peak, yielding a K_{eq} of 6.6 nM. A clear plateau was observed at saturation with no fluorescence change observed for [TBP] > 275 nM. In contrast to the FRET results, binding of the singly labeled 14_{dpx}*F to TBP (320 nM) resulted in an 8−10% *increase* in the 520 nm peak, with no further change up to 640 nM TBP.

The fluorescence lifetime measurements in all cases gave phase shift and modulation responses that fit very well to a biexponential decay model (Table 1), with χ^2 varying from 0.12 to 0.87. The fluorescein emission in the singly labeled 14*F duplex was changed slightly upon binding to TBP; the 6% decrease in the integrated emission intensity ($\sum\alpha_i\tau_i$) presumably derives from a change in the local environment of the fluorescein with a consequent increase in the rate of internal conversion (k_i). This result implies that the 8−10% increase in the fluorescein peak intensity observed for the singly labeled 14_{dpx}*F in the steady state was due primarily to a change in static quenching. In contrast, the integrated intensity of the doubly labeled R*14_{dpx}*F was decreased by 41% upon binding to TBP, in very good accord with the change in steady state emission. This agreement between the steady state emission and the lifetime integrated intensities suggests that the former is reflecting primarily a change in the separation of the two fluorophores rather than a trivial change in static quenching. From previous studies, it is clear that one can draw such a conclusion from steady state measurements only in retrospect, after confirmation from analysis of lifetime measurements (Parkhurst & Parkhurst, 1995b).

The distance distribution for the free R*14_{dpx}*F, with $P(R)$ modeled as a shifted Gaussian, was well-described by values for $\bar{R}$ and σ of 56.50 ± 0.04 and 8.96 ± 0.14 Å, respectively. When the R*14_{dpx}*F was bound to TBP, the distribution broadened slightly (σ = 11.56 ± 0.04 Å), while $\bar{R}$ decreased to 46.79 ± 0.02 Å (Figure 2). The estimated standard deviations for $\bar{R}$ and σ are quite small. The actual 95% confidence region for the parameters, however, must be considered to extend ±4σ on each side of the reported $\bar{R}$ or σ value, since the parameter value itself could be located at the extremes of the confidence ellipse; the values reported for $\bar{R}$ and σ have therefore been determined to about ±0.1 Å. Two separate procedures were used to assess the validity of the analytically derived $P(R)$ values. First, molecular modeling (Insight, Biosym Technologies, San Diego, CA) was used to construct the R*14_{dpx}*F structure, consistent with that of B-DNA (Figure 3A). This structure was superimposed onto that of the 14-mer bound to TBP in the published cocrystal structure (Kim, J. L., et al., 1993), and the distance between dyes was manipulated to be 46.8 Å, the observed

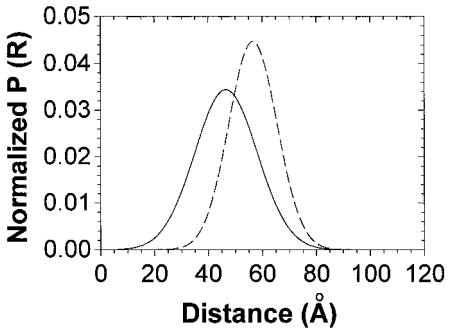

FIGURE 2: $P(R)$s for the R*14_{dpx}*F free (− −) and bound to TBP (—). The sine and cosine Fourier transforms of the frequency response from 4−208 MHz were recovered to within experimental error for the free R*14dpx*F; for the bound R*14_{dpx}*F, the error was ~3 times greater but rapidly approached the level of experimental error with truncation of high frequencies, with almost no change in σ and R.

mean 3′−5′ distance (Figure 3B). The distance was measured between the centers of the transition moments for the two dyes, assuming that the transition moment vector was directed between the two nitrogen atoms in the rhodamine and between the corresponding two oxygen atoms in fluorescein. The linker arms were then manipulated to obtain maximum and minimum interdye distances according to the constraints of the modeling program. These distances were 12.5 and 71.5 Å, respectively, in very good agreement with the extreme ends of the experimental $P(R)$. In this modeling, *only* the linker arms were allowed to move; no allowance was made for subtle changes in the duplex or the protein.

In the second procedure, $P(R)$ values for the free and TBP-bound R*14_{dpx}*F were obtained using Monte Carlo simulations. Maximum and minimum tether lengths to the 3′- and 5′-oxygens were determined using molecular modeling; these were, for fluorescein, 16.7 and 9.5 Å, respectively, and, for rhodamine, 20.0 and 9.0 Å, respectively. The dyes were allowed to rotate in a space defined by the frustum of a spherical "cone" with the apical half-angle ranging from 80 to 135°, and with the cone axis oriented 45° from the local DNA cylinder axis and in the plane defined by the cylinder axis and the radius of the cylinder to the 3′- or 5′-oxygen. Coordinates for the distorted DNA bound to TBP were taken from the crystallographic data (Kim, J. L., et al., 1993). Contacts between the tether termini and the cylinder <3.5 Å were excluded. The interdye distance was evaluated for 10 000 random points over a grid of cone angles and tether lengths that satisfied the geometric constraints. The simulated $P(R)$ for the bound case had values for $\bar{R}$ and σ of 46.7 and 10.5 Å, respectively, for cone angles of 135 Å for each dye tether, in excellent agreement with the observed distribution. In contrast, for the R*14_{dpx}*F alone, a minimum average interdye distance ($\bar{R}$) of 49.3 Å was found only for a very narrow range of cone angles (fluorescein, 80°, and rhodamine, 135°), demonstrating that the $\bar{R}$ of 46.8 Å observed for the bound R*14_{dpx}*F could derive *only* from a distortion of the B-DNA structure.

The kinetic course of the reaction was monitored using the stopped flow fluorimeter, with a dead time for the instrument determined to be 1.8 ms for the driving pressure of 35 psi employed in these experiments. A fast phase was *not* present with emission monitored at 200 μs intervals (Figure 4). The kinetic curve for the reaction of the R*14_{dpx}*F with 825 nM TBP is shown in Figure 5. Pseudo-

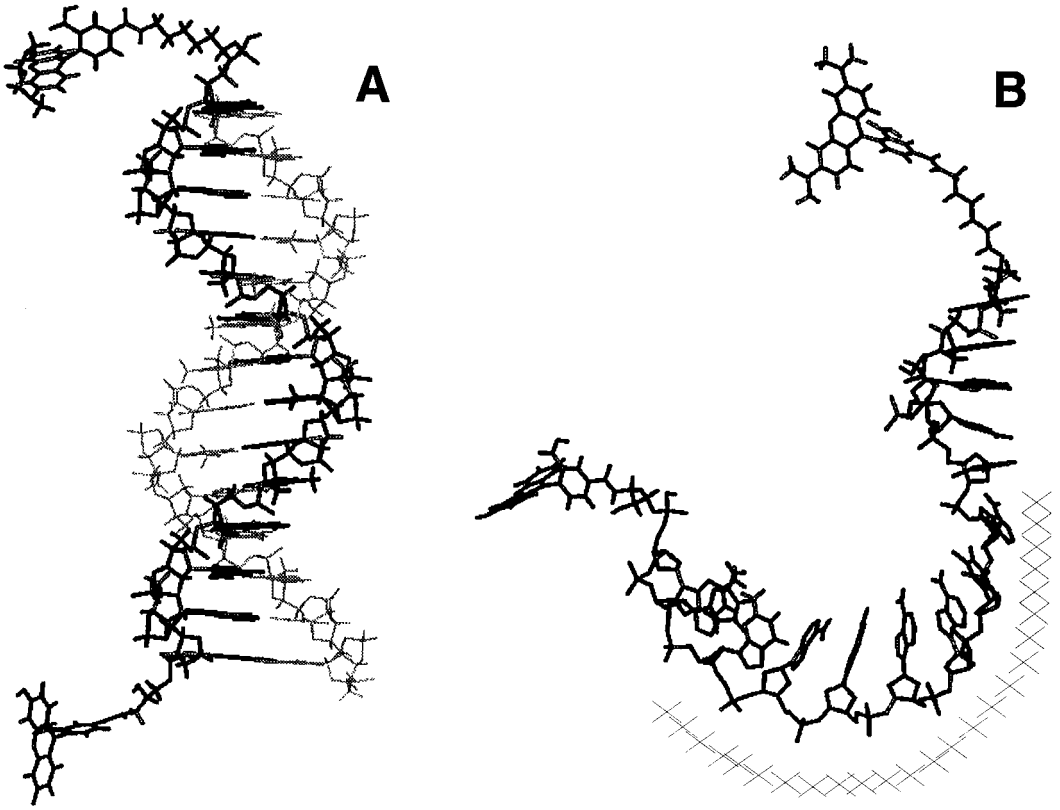

FIGURE 3: Structures obtained from computer modeling of the R*14$_{dpx}$*F free (A) and TBP-bound (B). In B, the complementary strand has been omitted for clarity and the TBP interface is shaded.

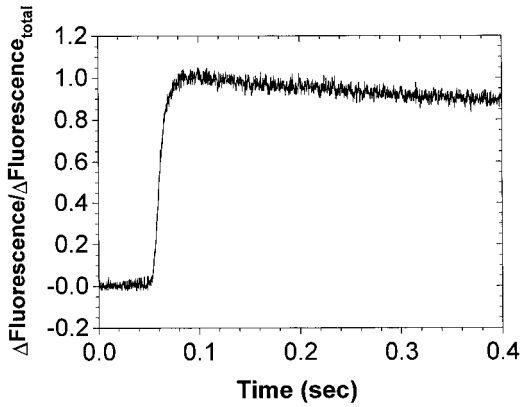

FIGURE 4: Stopped flow kinetic data, collected from 0−400 ms, for 20 nM R*14$_{dpx}$*F reacting with 275 nM TBP, showing the absence of a fast phase. The data were normalized after subtraction of the background voltage.

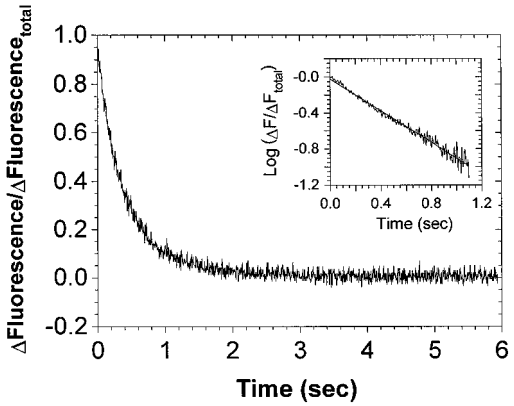

FIGURE 5: Stopped flow kinetic data for 20 nM R*14$_{dpx}$*F reacting with 825 nM TBP. The kinetic curves for 138 nM TBP (0−81 s) and 275 nM TBP (0−40 s) had essentially this same shape after corrections for base line voltage and photobleaching. A semilogarithmic plot (inset) was constructed from the corrected kinetic data out to $4t_{1/2}$ and fit by linear regression. The value for the pseudo-first-order rate constant was obtained from the slope of the fitted line.

first-order rate constants of 1.99 ± 0.27, 0.56 ± 0.01, and 0.35 ± 0.01 s^{-1} were obtained for 825, 275, and 138 nM TBP, respectively. The correlation coefficient for the regression analysis averaged 0.98 ± 0.01 for all curves and was slightly better at 825 nM TBP; these coefficients reflected a subtle lack of fit which was more apparent in the semilog plot (Figure 5 inset). Overall, the quality of the fits and the linearity of the pseudo-first-order constants with [TBP] were consistent with simple second-order behavior with $k_a = (2.4 \pm 0.3) \times 10^6$ M^{-1} s^{-1}. The amplitude of the change in fluorescein emission intensity for the kinetic curves, determined after corrections for base line voltage and photobleaching, was 36−38% and was independent of [TBP].

When the singly labeled 14$_{dpx}$*F was made to flow against TBP (275 nM after mixing), the emission *increased* slightly (∼3%), as in the static measurements, in the first 1.5 s of the reaction and then began to slowly decay at a rate that was identical, within experimental error, to the rate of photobleaching of fluorescein in the 14$_{dpx}$*F−TBP complex. The initial increase was consistent with that observed in the steady state measurements upon binding of the 14$_{dpx}$*F to TBP, and 1.5 s is $\sim t_{1/2}$ for the reaction observed with the R*14$_{dpx}$*F. The amplitude of the increase was less than that observed in the static measurements due to the simultaneous decrease in fluorescein emission from photobleaching.

DISCUSSION

The value of K_{eq} determined by FRET is in good agreement with the value 9.3 ± 0.6 nM determined by DNase

I "footprinting" of the major late promoter within a DNA restriction fragment under identical experimental conditions (M. Brenowitz, V. Petri, and E. Jamison, unpublished data). It is also consistent with the value of K_{eq} determined by Perez-Howard et al. (1995) using an identical 14-mer that was singly labeled with 5′-*x*-rhodamine to follow fluorescence anisotropy changes as a function of TBP binding when the temperature dependence of the TBP binding reaction is considered [*e.g.* Petri et al. (1995)]. (As noted by these authors, the anisotropy assay is sensitive to TBP binding but not to DNA bending.) The close correspondence of the results obtained using the R*14_{dpx}*F oligonucleotide and longer restriction fragments provides evidence that the doubly labeled oligonucleotide encompasses most, if not all, of the determinants of sequence-specific TBP binding.

The sensitive response of the R*14_{dpx}*F probe to changes in the fluorescein environment and to the 5′−3′ distance of the oligonucleotide makes it an excellent probe for observing DNA bending during the TBP binding reaction. The agreement of the static steady state and lifetime measurements confirms that the kinetic studies monitored the course of the interaction as the DNA probe bound to TBP and not trivial changes in static quenching. This conclusion is supported by two additional lines of evidence. First, there is excellent agreement between the analytically derived distance distributions, $P(R)$, for the 5′−3′ distance and the published duplex−TBP cocrystal structure. Second, Monte Carlo simulations demonstrated that the $\bar{R}$ and σ values obtained from the solution studies are completely consistent with the crystallographic data and can derive only from distortions of the B-DNA structure.

The molecular modeling of the distance distributions was done using the coordinates for the *A. thalania* TBP2. The DNA distortion is comparable in the two crystal structures that have been solved for TBP−DNA complexes, the *A. thalania* TBP2 (Kim, J. L., et al., 1993), which naturally lacks an extensive N-terminal domain, and the C-terminal domain of *S. cerevisiae* TBP (Kim, Y., et al., 1993). Since the experimentally determined distance distributions were obtained using the full length *S. cerevisiae* TBP, the very good agreement between the experimentally derived and calculated distance distributions suggests that the conformation of the DNA binding site of the native *S. cerevisiae* TBP−DNA complex in solution is comparable to that observed in the crystal structures.

Comparison of the stopped flow kinetic response of 14_{dpx}*F and R*14_{dpx}*F with TBP confirms that the decrease in fluorescence emission intensity for R*14_{dpx}*F arises exclusively from FRET. That the entire change in amplitude observed in the static steady state measurements is accounted for in the kinetic curves confirms that the latter fully represent the DNA−TBP interaction. Despite careful examination, no very fast phase was observed for the TBP−promoter association reaction. (With the experimental conditions of this study, approximately 60% of a reaction with a rate constant on the order of 10^9 M^{-1} s^{-1} would be observable if it were present.)

Several conclusions with respect to the mechanism of the TBP−promoter interaction can be drawn from these results. First, the association kinetics are second-order. Second-order behavior for the binding of promoter to TBP was first reported by Hoopes et al. (1992) and recently supported by Perez-Howard et al. (1995) and Petri et al. (1995). Second, there exists no detectable fast step in the reaction pathway beyond that for the diffusion-limited formation of the transient encounter complex that is the initial step in all bimolecular reactions in solution. Third, TBP−promoter binding and DNA bending occur simultaneously during the formation of the TBP−promoter complex over this range of TBP concentrations. Our results clearly rule out a reaction mechanism where the diffusion rate-limited binding of TBP

$$\text{TBP} + \text{DNA} \xrightarrow{k_+} \text{TBP}\cdot\cdot\text{DNA} \xrightarrow{k_a} \text{TBP}-\text{DNA}_{final}$$

with DNA results in the formation of a stable "encounter complex", TBP··DNA, that slowly isomerizes to the final bent DNA−TBP complex. If the fluorescein emission of the R*14_{dpx}*F probe changed in the first step, then a fast phase would have been observed for the reaction. Alternatively, if the fluorescein emission of the R*14_{dpx}*F probe remained *unchanged* as TBP and DNA bound to form TBP··DNA, then the subsequent slow isomerization, k_a, would follow *first-order* kinetics. Furthermore, no fast phase was observed for binding of the singly labeled 14_{dpx}*F to TBP; the only change observed with this probe occurred in the same time frame as that for the association of R*14_{dpx}*F to TBP. An initial fast phase was also not detectable by either stopped flow footprinting of TBP to a restriction fragment (Petri et al., 1995) or stopped flow anisotropy that monitored the binding (but not bending) of a 14-mer to TBP (Perez-Howard et al., 1995). These three stopped flow data sets are clearly incompatible with the two-step model proposed above.

The simplest model that is consistent with our results requires one additional step with the rate constant k_-:

$$\text{TBP} + \text{DNA} \underset{k_-}{\overset{k_+}{\leftrightarrow}} \text{TBP}\cdot\cdot\text{DNA} \xrightarrow{k_a} \text{TBP}-\text{DNA}_{final}$$

where TBP and DNA are in rapid equilibrium with the transient encounter complex TBP··DNA. Then, the rate of formation of TBP−DNA_{final} is a second-order process with a rate equal to k_2[TBP][DNA], and $k_2 = (k_+/k_-)k_a$. In this model, formation of the transient encounter complex TBP··DNA would not be detectable due to the very low steady state concentration. For the encounter complex to proceed along the reaction pathway to the TBP−DNA_{final} complex, a large activation barrier, which presumably derives from the DNA bending, must be overcome; it is the height of this barrier that accounts for the relatively low value of 2.4×10^6 M^{-1} s^{-1} that we have obtained for the second-order rate constant, k_2. Hoopes et al. (1992) arrived at the same model on the basis of a low value for the second-order association constant determined from gel mobility shift studies and, from that result, a prediction of an initial rapid equilibrium.

If the height of the activation barrier of the TBP−promoter interaction is attributable to a DNA conformational change, then a refinement of this model is that the unbound DNA exists as a *distribution* of DNA structures, $DNA_i \rightleftharpoons DNA_j \rightleftharpoons DNA_k$ ..., with the DNA conformers in equilibrium in a submillisecond time regime. The relatively slow rate of binding would then derive partially from the small fraction of the free DNA that at any time would be in the appropriate conformation (perhaps slightly prebent) to facilitate binding to TBP. The time-dependent binding of TBP to promoters

observed in our studies would then reflect the conversion of unbound and predominantly B-DNA to the final bent DNA−TBP complex.

In the most general sense, our model suggests a correlation between DNA bending and the kinetics of the TBP−promoter interaction. The recently published studies of Hawley and co-workers (Starr et al., 1995) established a correlation between the degree of DNA bending (as assayed by the electrophoretic circular permutation assay) in the TBP−promoter complexes with the rate of dissociation for a series of promoter sequences. The absence of either association rates or an equilibrium constant (from which the rate of association could be calculated) leaves open the question of whether there exists a similar relationship between the DNA bend and the rate-limiting step of the reaction. Alternatively, the formation of the DNA bend itself could be rate-limiting. If so, the prediction would be that the **rate of association** of TBP would be facilitated when binding a promoter prebent toward the major groove and inhibited by prebending toward the minor groove. Such an effect has been observed for the C-terminal domain of yeast TBP (Parvin et al., 1995). However, the concurrent effect on the rate of dissociation resulting from the prebending of the DNA precludes a simple interpretation of these data.

Further questions are raised by the observation of comparable DNA bends in cocrystal structures of *Arabidopsis* TBP complexed with a series of DNA sequences (S. Burley, personal communication) that include several sequences analyzed in the above-mentioned circular permutation studies. Since the studies described herein have established the consistency of the DNA bend observed in solution and in the crystal structures for the major later promoter, the source of this discrepancy is not clear. It is possible that TBP binding and DNA bending may be separable if the kinetics are followed over a range of TBP concentrations, temperature, and promoter sequences. The doubly labeled probe and associated energy transfer provide a direct and powerful means for resolving these questions. Another issue of great interest is the effect of TBP-associated protein factors (TAFs) on the TBP−promoter interaction; that issue is currently under investigation using the R*14_{dpx}*F and FRET.

ACKNOWLEDGMENT

We thank E. Jamison for preparation of the TBP, Dr. C. Ross for computer modeling, and Prof. S. Burley for making available to us the crystallographic coordinates for the structure of DNA−TBP for use in computer modeling.

REFERENCES

Cheung, H. C. (1991) in *Topics in Fluorescence Spectroscopy* (Lakowicz, J. R., Ed.) Vol. 2, pp 157−171, Plenum Press, New York.

Hoopes, B. C., LeBlanc, J. F., & Hawley, D. K. (1992) *J. Biol. Chem. 20*, 11539−11547.

Horikoshi, M., Bertuccioli, C., Takada, R., Wang, J., Yamamoto, T., & Roeder, R. G. (1992) *Proc. Natl. Acad. Sci. U.S.A. 89*, 1060−1064.

Kahn, J. D., & Crothers, D. M. (1992) *Proc. Natl. Acad. Sci. U.S.A. 89*, 6343−6347.

Kahn, J. D., Yun, E., & Crothers, D. M. (1994) *Nature 368*, 163−166.

Kim, J. L., & Burley, S. K. (1994) *Struct. Biol. 1*, 638−653.

Kim, J. L., Nikolov, D. B., & Burley, S. K. (1993) *Nature 365*, 520−527.

Kim, Y., Geiger, J. H., Hahn, S., & Sigler, P. B. (1993) *Nature 365*, 512−520.

Lakowicz, J. R., Gryczynski, I., Cheung, H. C., Wang, C.-K., Johnson, M. L., & Joshi, N. (1988) *Biochemistry 27*, 9149−9160.

Lee, D. K., Horikoshi, M., & Roeder, R. D. (1991) *Cell 67*, 1241−1250.

Martin, K. D., & Parkhurst, L. J. (1990) *Biochemistry 29*, 5718−5726.

Parkhurst, K. M., & Parkhurst, L. J. (1995a) *Biochemistry 34*, 285−292.

Parkhurst, K. M., & Parkhurst, L. J. (1995b) *Biochemistry 34*, 293−300.

Parkhurst, K. M., Hileman, R. E., Saha, D., Gupta, N. K., & Parkhurst, L. J. (1994) *Biochemistry 33*, 15168−15177.

Parvin, J. D., McCormick, R. J., Sharp, P. A., & Fisher, D. E. (1995) *Nature 373*, 724−727.

Perez-Howard, G. M., Weil, P. A., & Beechem, J. M. (1995) *Biochemistry 34*, 8005−8017.

Petri, V., Hsieh, M., & Brenowitz, M. (1995) *Biochemistry 34*, 9977−9984.

Starr, D. B., & Hawley, D. K. (1991) *Cell 67*, 1231−1240.

BI9530301